JOURNAL OF CATALYSIS 21, 336–348 (1971)

Chemisorption Studies by Chromatography—Hydrogen on Copper-Zinc Oxide

MOTOYUKI SUZUKI* AND J. M. SMITH

University of California, Davis, California

Received August 21, 1970

Equilibrium and kinetics of the chemisorption of hydrogen on a Cu-ZnO catalyst were studied at constant surface coverage by a chromatographic technique. Pulses of deuterium were introduced into a stream of hydrogen fed to a bed of catalyst particles, and the moments of the effluent peak were analyzed to determine the equilibrium isotherm and the rate parameters in the bed. At the conditions of the experiments, mass transfer resistance from gas to catalyst particle and within the porous particle were negligible. Axial dispersion was unusually significant, apparently due to nonuniform void regions caused by shrinkage of the catalyst particles. Rates were obtained from 150 to 250°C and at hydrogen pressures from 45 to 780 mm. At the equilibrium conditions of the experiments, adsorption and desorption rates were equal. These rates were found to increase with hydrogen pressure, even though the surface coverage remained essentially constant.

NOMENCLATURE

C_{D_2}	concentration of D_2 in gas phase, g-moles/cm³
C_d	concentration of deuterium, as D_2, defined by Eq. (2), g-moles/cm³
C_{HD}	concentration of HD in gas, g-moles/cm³
C_t	total concentration of hydrogen plus deuterium, g-moles/cm³
D_e	intraparticle diffusivity [cm²/min]
D	molecular diffusivity, cm²/min
E_A	axial dispersion coefficient, cm²/min
H	defined by Eq. (12), min
d_p	particle diameter, cm
H_0	defined by Eq. (13)
$HETP$	height equivalent to a theoretical plate, cm
K^*	pseudo adsorption equilibrium constant, defined by Equation (5), cm³/g
k^*	rate constant defined by Eq. (4) cm³/(g) (min)
k_f	mass transfer coefficient, cm/min
n_t	concentration of adsorbed hydrogen plus adsorbed deuterium, g-mole/g; n_∞ = concentration corresponding to total sites.
n_d	concentration of adsorbed deuterium, g-moles/g
p	pressure, mm Hg
P_e	axial Peclet number
q	tortuosity factor in the bed
Q	volumetric flow rate through the bed, cm³/min
R	total rate of adsorption or desorption, g-moles/(g)(min)
R_{D_2}	net rate of adsorption of deuterium as D_2, g-mole/(g)(min)
r	radial position in particle, cm
r_0	radius of particle, cm
T	temperature, °K
t	time, min
t_0	injection time of pulse, min

* On leave from Institute of Industrial Science, University of Tokyo.

V_c	volume of connecting lines between detector and bed, cm³
v	interstitial velocity of gas in the bed, cm/min
z	axial position, in the bed, cm; L = bed length

Greek Letters

α	interparticle void fraction in the bed
β	porosity of the catalyst particles
δ_0	defined by Eq. (8)
δ_1	defined by Eq. (9)
μ_1	first absolute moment for the bed, min
μ'_2	second central moment for the bed, (min)²
$(\mu_1)_{exp}$, $(\mu'_2)_{exp}$	moments determined from experimental chromatographs, as defined by Eqs. (10) and (11)
$\phi(\mu_1)$	first moment function defined by Eq. (18), min
ρ_p	density of particle, g/cm³

Introduction

Recent developments (*1*, *2*) in linear nonequilibrium chromatography make it possible to determine chemisorption rates on porous catalysts. The theory relates moments of the concentration peak at the outlet of the column, packed with catalyst particles, to the rate constants for diffusion and adsorption. Since chemisorption isotherms are nonlinear, the equations are intrinsically nonlinear. However, by introducing a pulse of an isotope into a carrier of the adsorbing gas (e.g., D_2 in a carrier of H_2), it is possible both to linearize the equation and to measure the rate constants at constant surface conditions corresponding to saturation with respect to the carrier.

In the work reported here, chemisorption rates and equilibrium constants were determined for hydrogen on a Cu-ZnO water gas–shift–reaction catalyst from 150–250°C. In contrast to the earlier studies (*1*, *2*), experiments were carried out at various hydrogen pressures from 45–780 mm Hg. This additional data provided information about the kinetics of adsorption.

Isotope (Tracer) Method

In the experiments, hydrogen is flowing continuously through a bed of catalyst particles at constant temperature and pressure. Under these equilibrium conditions, the surface coverage is constant, and the rates of adsorption and desorption are equal (designated as R). Suppose deuterium is introduced as a tracer to the hydrogen stream, keeping the total concentration of $H_2 + D_2$ constant. If the isotope effect is neglected, the total rates will not change, but it is possible to distinguish the molecules of D_2 and HD from those of H_2 in the detector (thermal conductivity cell) at the outlet of the bed. The rate of adsorption of deuterium is equal to R multiplied by the mole fraction, C_d/C_t, of deuterium in the gas. Similarly, the rate of desorption will be R multiplied by the fraction of the adsorbed atoms which are deuterium. Therefore, the net rate of adsorption of the tracer is given by

$$R_{D_2} = R\frac{C_d}{C_t} - R\frac{n_d}{n_t} = \frac{R}{C_t}\left(C_d - \frac{1}{n_t/C_t}\,n_d\right). \tag{1}$$

It may be that near equilibrium will be obtained for the exchange reaction $H_2 + D_2 = 2HD$. In order for the deuterium concentration C_d to be independent of whether the deuterium in the gas phase is present as D_2 or HD, C_d is defined as

$$C_d = \tfrac{1}{2}C_{HD} + C_{D_2}. \tag{2}$$

Since the total concentration C_t of hydrogen plus deuterium and the total adsorbed concentration n_t are constant, Eq. (1) is linear in C_d and n_d.

Equation (1) may be rewritten, in terms of quantities measured directly from the chromatographic data, as

$$R_{D_2} = k^*\left(C_d - \frac{1}{K^*}\,n_d\right), \tag{3}$$

$$k^* = \frac{R}{C_t}, \text{ and} \tag{4}$$

$$K^* = n_t/C_t. \tag{5}$$

Once k^* and K^* are determined, R can be obtained from Eq. (4). Both k^* and K^* are the same throughout the bed. K^* is not the adsorption equilibrium constant in the usual sense but simply the ratio of n_t to C_t at a single point on the nonlinear isotherm. Experiments at different total concentrations (pressures of hydrogen) and temperature give different values of k^* and K^*. These results determine the effect of pressure and temperature upon the rate and the adsorption isotherm.

Method of Analysis

The differential mass balances and boundary and initial conditions, describing the movement of tracer through the bed, have been presented in detail elsewhere (*1*). Also presented were the relations of the solutions of these equations to the moments of the concentration peak of deuterium in the effluent from the bed. The results in terms of the difference between the moments of the effluent and inlet peaks are as follows:

$$\Delta\mu_1 = \mu_1 - \frac{t_0}{2} = \frac{z}{v}(1 + \delta_0), \tag{6}$$

$$\Delta\mu_2 = \mu'_2 - \frac{1}{12}t_0^2 = \frac{2z}{v}\left[\delta_1 + \frac{E_A}{\alpha}(1 + \delta_0)^2\frac{1}{v^2}\right], \tag{7}$$

where

$$\delta_0 = \frac{1-\alpha}{\alpha}\beta\left(1 + \frac{\rho_p K^*}{\beta}\right), \text{ and} \tag{8}$$

$$\delta_1 = \frac{1-\alpha}{\alpha}\beta\left[\frac{\rho_p}{\beta}\frac{(K^*)^2}{k^*} + \frac{r_0^2\beta}{15}\left(1 + \frac{\rho_p}{\beta}K^*\right)^2\left(\frac{1}{D_c} + \frac{5}{k_f r_0}\right)\right]. \tag{9}$$

The mass balances include mass transfer in the interparticle space by bulk flow (at gas velocity v) and axial dispersion (according to diffusivity E_A), transport from gas to particle (transfer coefficient k_f), intraparticle transport (effective diffusivity D_e) and adsorption at an interior site governed by Eq. (1). Equations (6–9) relate the four rate parameters E_A, k_f, D_e, k^*, to the moments, which may be determined experimentally. The equations are for isothermal conditions, spherical particles of radius r_0, and suppose no radial gradients in the bed.

The first absolute moment is defined as

$$(\mu_1)_{\text{exp}} = \frac{\int_0^\infty tC_d(L,t)\,dt}{\int_0^\infty C_d(L,t)\,dt}, \tag{10}$$

and the second, central moment as

$$(\mu'_2)_{\text{exp}} = \frac{\int_0^\infty (t-\mu_1)^2 C_d(L,t)\,dt}{\int_0^\infty C_d(L,t)\,dt}. \tag{11}$$

The thermal conductivity cell used to measure gas composition was operated so that hydrogen flowed through the reference side and the effluent peak through the sample side. Hence, the signal observed was proportional to the concentration of deuterium in the effluent. Since the concentration occurs in both numerator and denominator of Eqs. (10) and (11), the recorded effluent peaks can be used directly to evaluate the moments.

Equations (6) and (8) along with data for the first absolute moment were employed to evaluate K^*. Data for μ'_2 were obtained for several velocities and catalyst particle sizes. This information with Eqs. (7) and (9), allowed the contributions of axial dispersion and diffusion to be evaluated independently. Then the contribution of adsorption and, hence, k^* could be determined. The analysis is simplified by first dividing Eq. (7) by $[\Delta\mu_1/(z/v)]^2$, obtained from Eq. (6). The result is

$$H = \frac{\frac{1}{2z/v}(\Delta\mu_2)}{\left(\frac{1}{z/v}\Delta\mu_1\right)^2} = H_0 + \left(\frac{E_A}{\alpha}\right)\frac{1}{v^2}, \tag{12*}$$

where

$$H_0 = \frac{\delta_1}{(1+\delta_0)^2}. \tag{13}$$

* H is related to the plate theory of chromatography by the expression, $H = HETP/2v$.

The procedure we have used is to evaluate H_0 from the moments for different velocities using Eq. (12). Then δ_1 was determined from Eq. (13) and used with Eq. (9) to obtain k^*.

Equation (13) reduces to simpler forms for nonadsorbing (inert) and highly-adsorbed gases. For an inert gas, $K^* = 0$, so that

$$(H_0)_{\text{inert}} = \frac{\frac{1-\alpha}{\alpha}\beta^2 r_0^2}{\left(1+\frac{1-\alpha}{\alpha}\beta\right)^2}\left(\frac{1}{15D_e}+\frac{1}{3k_f r_0}\right) \quad (14)$$

When the gas is highly adsorbed, $\rho_p K^* \gg \beta$ or $\alpha/(1-\alpha)$, and Eq. (13) becomes

$$H_0 = \frac{\alpha}{1-\alpha}\left[\frac{1}{\rho_p k^*} + r_0^2\left(\frac{1}{15D_e}+\frac{1}{3k_f r_0}\right)\right] \quad (15)$$

Actually, the second condition implies only that the catalyst surface holds much more adsorbate than the inter and intraparticle gas volume. For most adsorption systems this condition is met. For example, numerical calculations show that, for normal values of α and β in packed beds, if $\rho_p K^* = 30$, the use of Eq. (15) in place of Eqs. (9) and (13) would introduce a maximum error of 10%. For all of the data reported here $\rho_p K^*$ varied from 33 to 610. Hence Eq. (15) was used.

Equations (12) and (15) demonstrate the additivity of the contributions of axial dispersion, gas-particle mass transfer, intraparticle diffusion, and adsorption, to the ratio H.

This additivity was shown earlier (*3*) for an infinite adsorption rate by assuming a Gaussian form of the effluent peak.

Experimental

Apparatus

The equipment was the same as a conventional gas chromatograph except that the separation column was replaced with the column of catalyst particles. A pulse of deuterium was introduced into the hydrogen stream (see Fig. 1) through a 7-port valve. The stream then flowed through one side of the thermal conductivity cell and the bed of catalyst particles. The effluent was passed through the other side of the

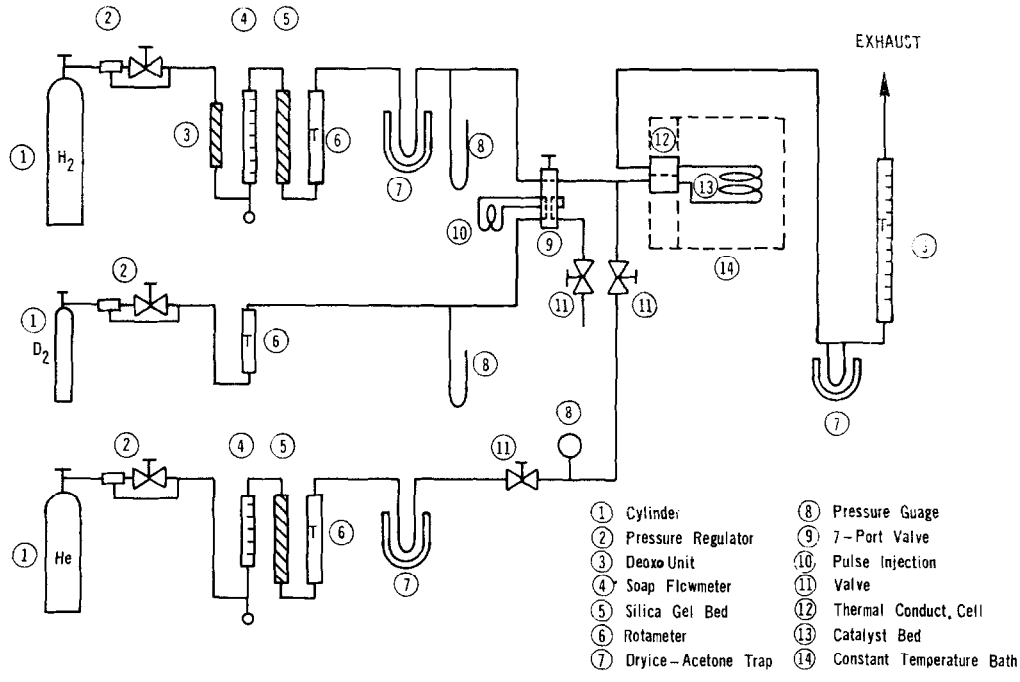

FIG. 1. Schematic diagram of apparatus.

cell. In this way, it was possible to measure the composition–time relationship for both the inlet and effluent peaks. The equipment was designed to minimize the volume in the lines between the detector and the bed. This volume was found to be 3.0 cm^3 by measuring the retention time of the deuterium pulse when the reactor was bypassed. The catalyst particles were packed in .635 cm nominal size, copper tubing to lengths between 29 and 99 cm. The bed was located in a constant temperature bath. By exchanging cylinders, it was possible to add pulses of helium or deuterium to the hydrogen stream.

Gases

The prepurified hydrogen (stated purity 99.95%) was passed through a Deoxo unit to remove traces of oxygen. Water in the hydrogen and helium streams was removed by dry ice-acetone baths and beds of silica gel. The purity of the helium was specified to be 99.99%, while the deuterium was technical grade (98% purity).

Catalyst Particles

The composition of the unreduced, commercial, water gas–shift–reaction catalyst (catalyst G-66B from the Chemetron Corporation) was 82.5 wt % zinc oxide and 16.5 wt % copper oxide. The original pellets were crushed and screened, and the properties of the particles so obtained are given in Table 1. The densities were measured in a Beckman air pycnometer using helium, and the pore volume and porosity (β) were calculated from the density data. The surface area was evaluated by passing several mixtures (of increasing nitrogen mole fraction) of helium and nitrogen through a bed of particles (Column II, see Table 2) maintained at liquid nitrogen temperature and measuring the amount of nitrogen adsorbed. Data were obtained before and after reduction of the catalyst particles. The 8.3% decrease in area appears to be due to shrinkage of the particles. The pore-volume distribution was determined by standard methods (nitrogen condensation and mercury penetration). The distribution curve showed that the catalyst had a monodispersed pore structure with a most-probable pore diameter of about 350 Å.

TABLE 1
PROPERTIES OF CATALYST

Composition (unreduced), wt %		
ZnO	82.5	
CuO	16.5	
Pore volume (cm^3/g)	0.24	(unreduced)
Particle density (g/cm^3)	2.35	(unreduced)
True density (g/cm^3)	5.29	(unreduced)
Porosity, β	0.56	(unreduced)
	0.60	(reduced)
Most probable pore diameter (Å)	350	(unreduced)
Surface area, ($m^2/g_{unreduced}$)	35.9	(unreduced)
	32.9	(reduced)

Before use the beds of catalyst particles were reduced in place by a two-step process: (1) passing a mixture of hydrogen and helium (of gradually increasing hydrogen content) through the bed for 10 hr at 240°C followed by, (2) a pure hydrogen flow for 10 hr at 255°C. Such reduction reduces all of the copper oxide to copper but has no effect on the zinc oxide. This is confirmed by the X-ray diffraction studies of Tsuchimoto and Morita (*4*) on similar catalysts prepared by reduction of $CuO \cdot ZnO$ with CO–H_2O mixtures at 250°C.

The reduced catalyst adsorbed oxygen from the air so rapidly that densities and the pore-volume distribution could not be measured. The properties shown in Table 1 are for unreduced particles. The porosity of the reduced catalyst was estimated indirectly by measuring the first moment (retention time) of a helium pulse in Column I. For this nonadsorbing gas, and by taking $\alpha = 0.45$ (Table 2), β could be calculated from Eqs. (6) and (8). The result was 0.60 in comparison with 0.56 obtained directly from the unreduced catalyst.

Bed Characteristics

The pertinent properties of the three packed beds, one for each particle size, are shown in Table 2. The average particle diameter assigned for each size was taken as the arithmetic average of the maximum and minimum sieve openings. The shrinkage of

TABLE 2
CHARACTERISTICS OF PACKED COLUMNS

	Column I	Column II	Column III
Range of sieve openings, (mm)	0.991–0.701	0.701–0.589	0.417–0.295
Ave. particle radius, (mm)	0.423	0.323	0.178
Column area, (mm^2)	0.19	0.19	0.19
Column diameter, (mm)	4.9	4.9	4.9
Packed length (unreduced)(cm)	79.0	99.0	29.0
Mass of catalyst, (g)(unreduced)	22.33	26.74	7.262
α (unreduced)	0.37	0.40	0.44
(reduced)	0.45	0.48	0.51

the packed volume due to reduction was measured for Column II. Following the runs with reduced catalyst, the packed length was measured after straightening and tapping the column. This length, 87.5 cm, compared with the length (after tapping) of 99 cm for the bed of unreduced particles gives a reduction of 12%. Using this reduction the relation between α for beds of reduced and unreduced particles is

$$(\alpha)_{\text{red.}} = 1 - 0.88\,[1 - (\alpha)_{\text{unred.}}] \quad (16)$$

For Column II, the value of α for the unreduced catalyst, as determined from the packed length, mass and particle density, was 0.40. The corresponding value of α for the bed of reduced particles calculated from Eq. (16) is 0.48. The values in Table 2 for the other columns were also calculated from Eq. (16). These results were used in the subsequent analysis of the data. Note that β is not needed in applying Eqs. (12) and (15).

Shrinkage due to reduction significantly increased the porosity in the bed and gave larger void regions between particles. The axial Peclet numbers obtained from the moment analysis suggest that the increased α values led to channeling.

Experimental Program

First, runs were made with helium pulses at 200°C and varying hydrogen rates to establish the influence of axial dispersion and intraparticle diffusion. These measurements were made with Column I. Next, for each column, deuterium pulses were introduced into a pure hydrogen stream and runs carried out at various flow rates, all at 200°C. This data gave additional information about axial dispersion and intraparticle diffusion, and also provided a set of k^* and K^* values for a hydrogen pressure of 780 mm. Finally, deuterium pulses were introduced into a stream of hydrogen and helium. By varying the composition of the hydrogen–helium mixture, it was possible to obtain k^* and K^* over a range of hydrogen pressure from 45–780 mm. These runs were made at 150, 175, 200, 225, and 250°C in Column III.

The volumetric flow rate of carrier gas was varied from about 35 to 125 cm^3/min (room temperature and 1 atm). This corresponded to a range of interparticle velocities from about 770 to 3100 cm/min for the runs at 200°C.

Typical Chromatographs

Figure 2 shows effluent chromatographic peaks for deuterium pulses in pure hydrogen for Column III at several temperatures and approximately the same velocity. Also shown is the inlet peak (at 250°C) at an attenuation 32 times larger than that for the effluent peak. Comparison of the two curves shows that the dispersion (width) of the inlet peak was negligible with respect to that of the effluent chromatograph of deuterium.

The lower limit of temperatures studied was determined by the extent of tailing. The curves in Fig. 2 illustrate the difficulty in obtaining accurate values of the second moment at temperatures below 175°C. While the curves show increasing dispersion as the temperature is decreased, and have increased second moments, the average

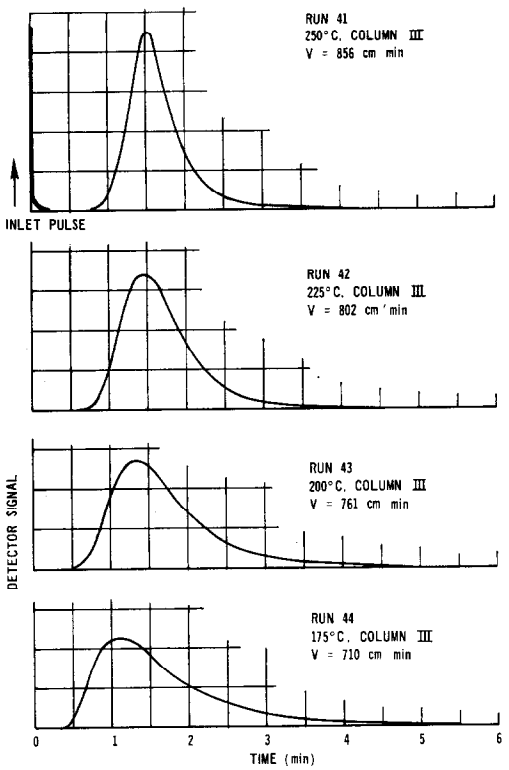

FIG. 2. Deuterium chromatographs at various temperatures.

retention time varies little from 250–170°C. Therefore, the amount adsorbed does not change much with temperature, as the subsequent analysis of first-moment data shows.

ANALYSIS OF FIRST-MOMENT DATA (HYDROGEN PRESSURE = 780 mm)

The moments of the deuterium peak applicable in Eqs. (6), (7), and (12) are those for the bed of particles, while the experimental moments obtained from Eqs. (10) and (11) include the effects of the volume in the lines connecting the detector and the bed. The first moments for the bed itself can be obtained from the experimental moments and the volume of the connecting lines (3.0 cm^3) using the equation

$$\Delta\mu_1 = [(\mu_1)_{\text{eff}} - (\mu_1)_{\text{inlet}}]_{\text{exp}} - \frac{V_c}{Q}. \quad (17)$$

Then Eqs. (6), (8) and (17) give

$$\phi(\mu_1) = \frac{\Delta\mu_1 - \frac{z}{v}\left(1 + \frac{1-\alpha}{\alpha}\beta\right)}{\frac{1-\alpha}{\alpha}} = (\rho_p K^*)\frac{z}{v} \quad (18)$$

A plot of ϕ vs z/v is shown for the data at 200°C in Fig. 3. From the slope of the line K^* can be calculated, and these results for all temperatures are given in Table 3. The amount adsorbed, obtained from Eq. (5) and K^*, is shown in Fig. 4. The nearly constant values of n_t indicate that the catalyst surface is essentially saturated with hydrogen from 150–250°C. This result is the same as those of Taylor *et al.* (*5–7*), who studied the adsorption of hydrogen on pure zinc oxide.

ANALYSIS OF SECOND-MOMENT DATA (HYDROGEN PRESSURE = 780 mm)

Axial Dispersion

Equation (12) shows that the contribution of axial dispersion to H must be evaluated before H_0, and then k^*, can be ascertained. Because of its unusual significance, apparently due to the shrinkage of the catalyst particles during reduction, axial dispersion was evaluated over a wide range of velocities from the helium-pulse data for comparison with the contribution obtained from the deuterium-pulse results.

In packed beds E_A is commonly expressed as a sum of a molecular diffusion (D) term and a term due to the velocity profile (function of Peclet number P_e),

$$E_A = \frac{\alpha D}{q} + \frac{2\alpha}{P_e}(r_0 v). \quad (19)$$

Figure 6a shows the moments from the helium-pulse data in the high velocity region plotted as H vs $1/v$. The values of H were calculated from Eq. (12) using Eq. (17) to obtain $\Delta\mu_1$. For $\Delta\mu_2$ the same form as Eq. (17) was used except no correction for V_c was necessary because the dispersion in this small volume was negligible. The line in Fig. 6a extrapolates to the origin. According to Eqs. (12) and (14) $H_0 = 0$, so that the value of H is entirely

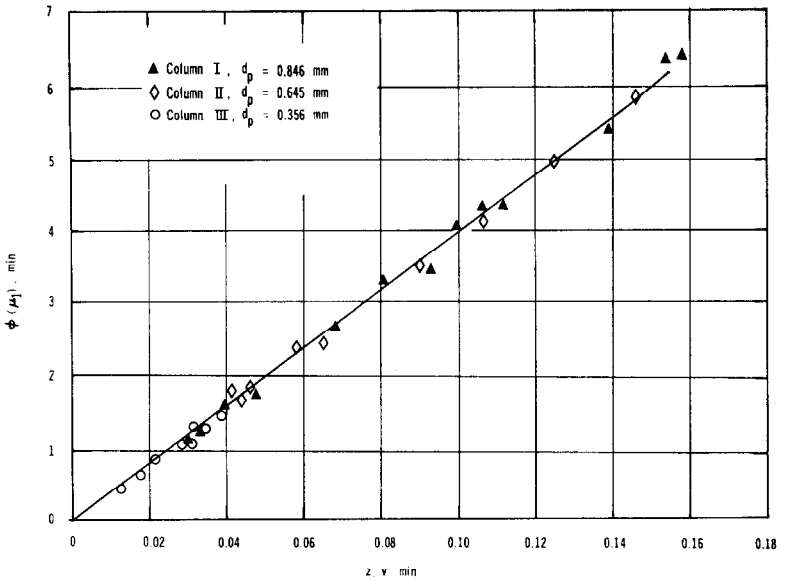

FIG. 3. First—moment data for deuterium.

due to axial dispersion. Thus, for these data, Eqs. (12) and (19) give

$$(H)_{\text{inert}} = \left(\frac{D}{q} + \frac{2}{P_e} r_0 v\right) \frac{1}{v^2} \qquad (20)$$

Since P_e is independent of velocity at high velocities, Eq. (20) suggests that $(H)_{\text{inert}}$ should be proportional to $1/v$ at low $1/v$. At low velocities the molecular diffusion term should be dominant so that $(H)_{\text{inert}}$ would be proportional to $(1/v)^2$. The helium-pulse data for a wide range of velocities follow these predictions as shown in Fig. 5. At $10^3/v < 7$, $(H)_{\text{inert}}$ is proportional to $1/v$, and the Peclet number obtained from Eq. (20) is $P_e = 0.071$. At

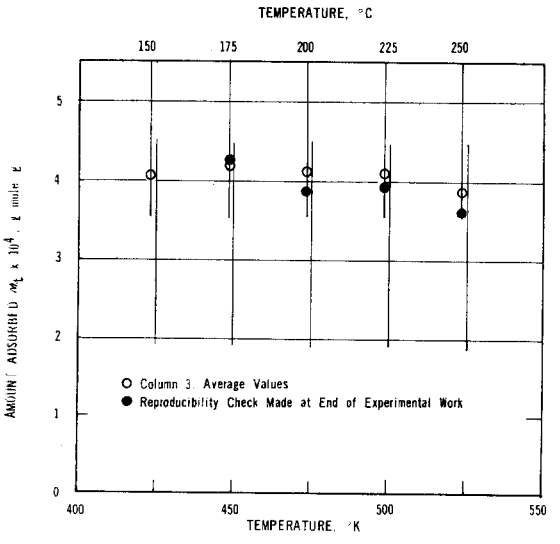

FIG. 4. Equilibrium adsorption for hydrogen on catalyst.

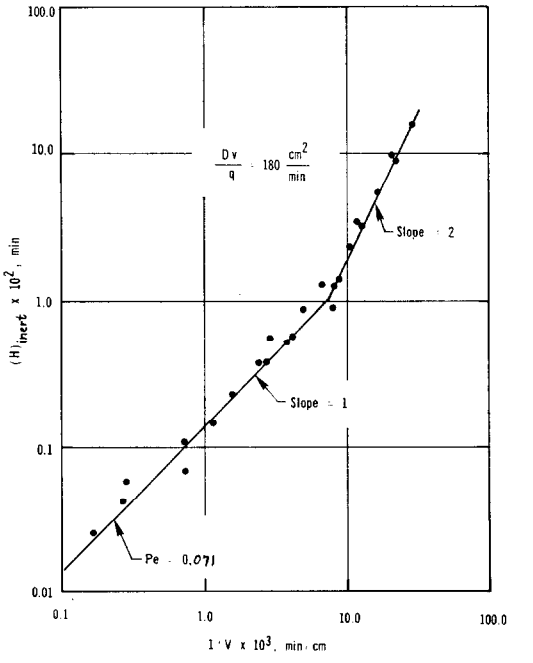

FIG. 5. H for Helium pulse vs $1/V$ at 200°C (Column 1).

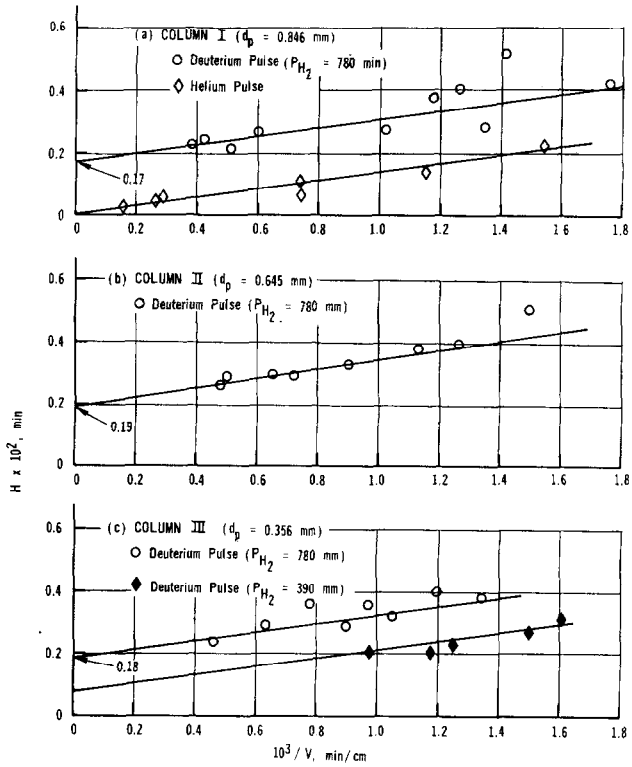

FIG. 6. H vs $1/V$ at 200°C, for all columns.

lower velocities, $(H)_{inert}$ is proportional to $1/v^2$, and this section of Fig. 5 gives $D/q = 180$ cm²/min. The corresponding tortuosity factor is $q = 0.87$. This lower than normal value may be due to heterogeneity in the void spaces around the catalyst particles after reduction.

Since the purpose of this work was to obtain rates of adsorption, the axial dispersion contribution to H was minimized by obtaining deuterium-pulse data in the high velocity range where H is proportional to $1/v$. The deuterium data were plotted vs $1/v$ and extrapolated to obtain H_0, as illustrated in Fig. 6a–c for the results at 200°C. The slopes of these lines also can be used to evaluate axial dispersion contributions. From Eqs. (12) and (19), the slope is equal to $2r_0/P_e$. The resulting Peclet numbers for the 200°C data are as follows:

Column	Peclet number
I, d_p = 0.846 mm	0.071
II, d_p = 0.645 mm	0.044
III, d_p = 0.356 mm	0.027

The value for Column I is the same as that obtained from the helium-pulse data. These Peclet numbers, while consistent, are much lower than expected from the theory of uniformly packed particles in a bed. The difference is presumably due to a severely nonuniform distribution of velocity in the bed caused by shrinkage of the particles. The values of P_e are approximately proportional to the particle diameter as reported by Klinkenberg *et al.* (*3*) and Perkins and Johnson (*8*).

Intraparticle and External Diffusion

Equation (15) states that the effects of intraparticle diffusion and gas-particle mass transfer on H_0 are a function of particle size. However, the experimental H_0 (obtained from the intercepts in Figure 6a–c) as shown in Fig. 7 are independent of particle radius. Therefore, the effects of both intraparticle and gas-particle mass trans-

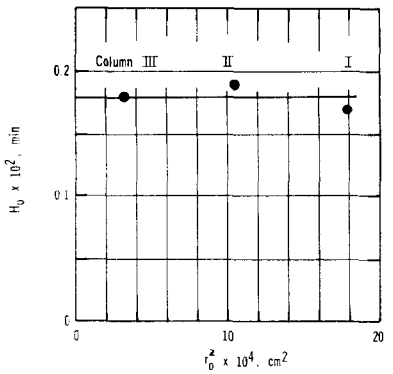

FIG. 7. H_0 vs r_0^2 (200°C).

port on the adsorption rate are negligible for the small particles used and the relatively slow adsorption rate for the Cu-ZnO catalyst. This conclusion is substantiated by the helium-pulse data shown in Fig. 6a. The zero intercept ($H_0 = 0$) for this inert system suggests [see Eq. (14)] that the diffusion effects are negligible. It may be noted that gas-particle mass transfer effects are usually insignificant for the small particles used in small chromatographic columns (*1*, *2*, *8*), but for high rates of adsorption, intraparticle diffusion can have a large effect (*1*) and even be dominant for physical adsorption (*9*).

Chemisorption Rates

For negligible diffusion effects, Eq. (15) reduces to

$$H_0 = \frac{\alpha}{1 - \alpha}\left(\frac{1}{\rho_p k^*}\right) \qquad (21)$$

From intercepts on the H vs $1/v$ plots, illustrated in Fig. 6, H_0 was evaluated over the whole temperature range from the Column III data. Then k^* was obtained from Eq. (21) and R from Eq. (4). The results are given in Table 3. The Arrhenius plot of the rates in Fig. 8 suggests an activation energy of 14.6 kcal/(g-mole). The deviation of the point at 150°C is likely caused by inaccuracies due to tailing of the chromatographs at this low temperature. Taylor and Strother (*6*) studied the rate of adsorption of hydrogen on zinc oxide alone as a function of surface coverage. At high coverages and in the temperature range of their work which most closely corresponded to ours (184–218°C), they reported an activation energy of 15.3 kcal/g-mole.

Earlier results for rates of adsorption of hydrogen on nickel (*1*) and on cobalt (*2*) catalysts supported on Kieselguhr were obtained at temperatures from —34 to 25°C. At 24°C these rates, believed to correspond to nonactivated adsorption, were 60×10^{-2} and 9.6×10^{-2} g-moles/(g)(min). These results are about two orders of magnitude greater than the rates given in Table 3 for Cu-ZnO despite the much lower temperature for the nickel and cobalt values.

ANALYSIS OF SECOND-MOMENT DATA (VARIABLE p_{H_2})

The second-moment data for deuterium pulses in mixtures of hydrogen and helium were treated in the same way as was done for the data at $p_{H_2} = 780$ mm. Runs were made in the high range of gas velocity so as to increase the accuracy of the inter-

TABLE 3

RATES OF ADSORPTION AT $P_{H_2} = 780$ mm Hg[a]

Temperature °C	Pseudo equilibrium constant K^* (cm^3/g)	Amount adsorbed $n_t \times 10^4$ (g mole/g)	Adsorption rate constant $k^* \times 10^{-2}$ cm^3/(g)(min)	Adsorption rate $R \times 10^2$ mole/(g)(min)
150	13.7	4.07	0.54	0.16
175	14.9	4.17	1.39	0.39
200	15.6	4.13	2.45	0.65
225	16.5	4.12	6.20	1.56
250	16.1	3.87	11.6	2.80

[a] From data taken in Column III.

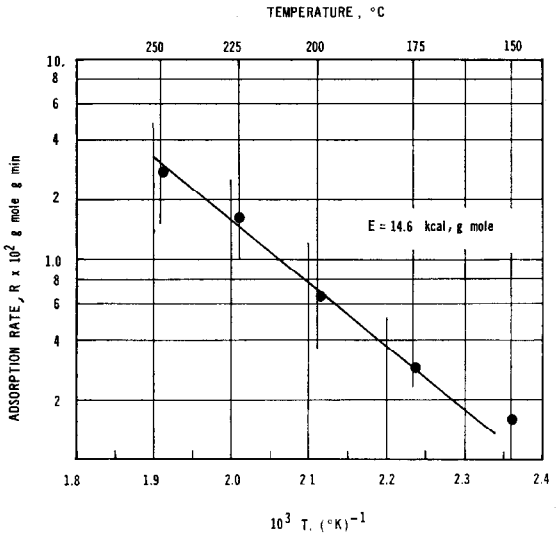

FIG. 8. Arrhenius plot for hydrogen adsorption.

cepts (H_0 values) in plots similar to Fig. 6. An illustration of the data is shown in Fig. 6c for $p_{H_2} = 390$ mm. Column III (smallest size particles) was employed so that negligible intraparticle and gas-particle mass transport effects were assured.

The first-moment results were used to evaluate K^* from Eq. (18). The amount adsorbed at equilibrium was then obtained from Eq. (5). The resulting n_t values are plotted vs p_{H_2} in Fig. 9 for 200 and 250°C. Results for other temperatures showed no significant differences from the 200 and 250°C values. Next, the first and second-moment information was employed to establish H and H_0, as described in the previous paragraph. Finally, k^* and R were obtained from Eqs. (21) and (4), and the rates are plotted vs. p_{H_2} in Fig. 10.

Figure 9 indicates that at $p_{H_2} > 45$ mm the surface is approaching saturation, since n_t changes little with either pressure or temperature. However, the gradual increase in n_t with hydrogen pressure suggests that some bare sites still exist. From the surface area obtained by nitrogen adsorption for the reduced catalyst (32.9 m²/g) and the amount of hydrogen adsorbed from Fig. 9, the concentration of surface sites can be estimated. Assuming that each site is occupied by a hydrogen atom, the number of sites per cm² is

$$\frac{(4.1 \times 10^{-4})(2)(6.023 \times 10^{23})}{(32.9 \times 10^{-4})} = 1.5 \times 10^{15}\ \text{cm}^{-2}.$$

This result is also evidence of near-saturation conditions since the concentration of active sites on oxide catalysts is normally taken to be of the order of 10^{15}/cm².

Kinetics of Adsorption

If chemisorption occurs by a dissociative mechanism,

$$H_2 + 2S = 2H \cdot S,$$

on the bare sites on the catalyst, the rates (R) of adsorption and desorption would be

$$R = k(n_\infty - n_t)^2 C_{H_2} = k' n_t^2. \quad (22)$$

If adsorption is non-dissociative,

$$R = k(n_\infty - n_t) C_{H_2} = k' n_t, \quad (23)$$

where n_∞ is concentration corresponding to the total sites active for adsorption. While n_t is nearly constant (Fig. 9) and approaching n_∞, the fractional change in

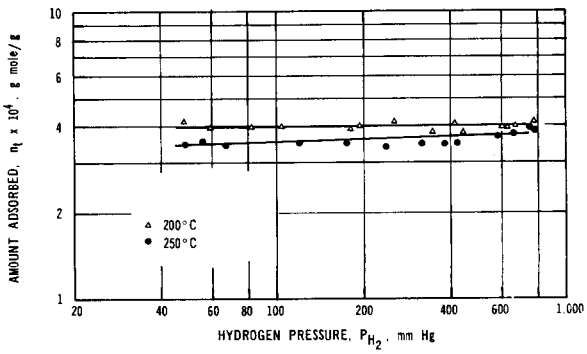

FIG. 9. Adsorption isotherms at 200°C and 250°C.

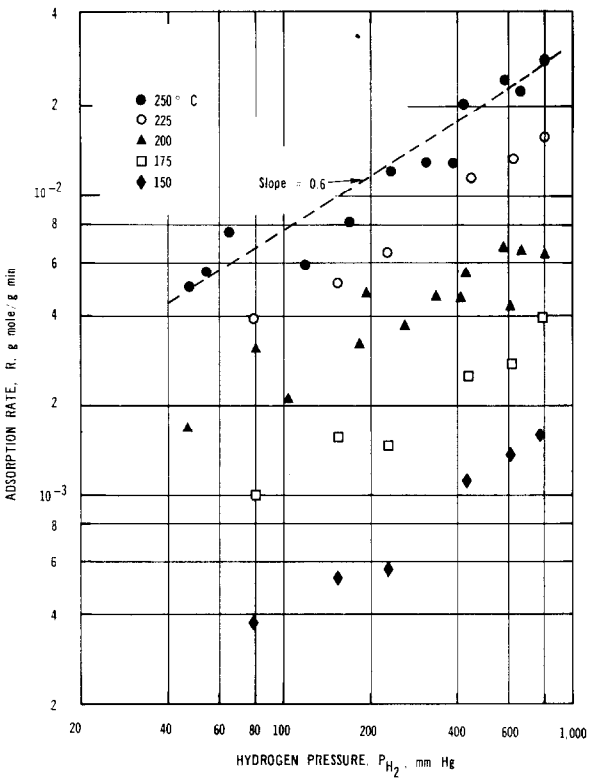

FIG. 10. Adsorption rate vs hydrogen pressure.

$n_\infty - n_t$ with p_{H_2} can be large and is unknown. Hence, the relation between adsorption rates and p_{H_2} in Eqs. (22) and (23) is unknown. However, the desorption forms of these equations show that R should be independent of p_{H_2}, because n_t is nearly independent of p_{H_2}. The data in Fig. 10, showing about 0.6 order with respect to p_{H_2}, are not in agreement with this conclusion. Equations (22) and (23) are based upon the assumptions that all sites are of equal activity and that there is no interaction between sites. It is unlikely that the complex sites on the Cu-ZnO particles satisfies either of these postulates, so that it is not surprising that the rate data do not fit Eqs. (22) and (23). As noted by Halpern (*10*), hydrogen adsorption rates are often found to 0.3–0.6 order with respect to hydrogen, and this is attributed to the involvement of weaker sites at higher pressures. A mechanism based upon the exchange of hydrogen between gas and chemisorbed phases, as postulated by Rideal (*11*),

$$H_2 + H \cdot S \rightarrow H \cdot S + H_2, \qquad (24)$$

would lead to rate equations for adsorption and desorption which are proportional to p_{H_2}. This result is in partial agreement with Fig. 10, but available data do not support the Rideal mechanism at above room temperature (*12*).

In conclusion, the results show that a ZnO-Cu catalyst for the water gas–shift reaction readily chemisorbs hydrogen from 150–250°C. The adsorption capacity is nearly constant over this temperature range and also independent of hydrogen pressure in the range 45–780 mm. Despite this latter fact, the rates of both adsorption and desorption increase with p_{H_2}.

ACKNOWLEDGMENTS

The financial support of the National Science Foundation, Grant GK-2243, is gratefully acknowledged. We also thank the Catalyst Division of Chemetron Corporation for providing the water gas–shift-reaction catalyst.

References

1. Padberg, G., and Smith, J. M., *J. Catal.* **12,** 172–182 (1968).
2. Adrian, J. C., and Smith, J. M., *J. Catal.* **18,** 57 (1970).
3. Klinkenberg, A., and Sjenitzer, F., *Chem. Eng. Sci.* **5,** 258 (1956).
4. Tsuchimoto, K., and Morita, T., *Kogyo Kagaku Zasshi* [*Bull. Chem. Soc. (Ind. Chem.) Jap.*] **70,** 665, 1473 (1967).
5. Taylor, H. S., and Sickmann, D. V., *J. Amer. Chem. Soc.* **54,** 602 (1932).
6. Taylor, H. S., and Strother, C. O., *J. Amer Chem. Soc.* **56,** 586 (1934).
7. Taylor, H. S., and Liang, S. C., *J. Amer Chem. Soc.* **69,** 1306 (1947).
8. Perkins, T. K., and Johnson, O. C., *Soc Petrol. Eng. J.* **3,** 70 (1963).
9. Schneider, P., and Smith, J. M., *AIChE J* **14,** 762 (1968).
10. Halpern, J., *Advan. Catal. Relat. Subj.* **11,** 345 (1959).
11. Rideal, E. K., "Concepts in Catalysis," pp 113–118. Academic Press, New York, 1968
12. Bond, G. C., "Catalysis by Metals," pp. 165–170. Academic Press, New York, 1962.